

## Cooperative scattering and radiation pressure force in dense atomic clouds

R. Bachelard,<sup>1</sup> N. Piovella,<sup>2</sup> and Ph. W. Courteille<sup>3</sup>

<sup>1</sup>*University of Nova Gorica, School of Applied Sciences, Vipavska 11c SI-5270 Ajdovscina, Slovenia*

<sup>2</sup>*Dipartimento di Fisica, Università Degli Studi di Milano, Via Celoria 16, I-20133 Milano, Italy*

<sup>3</sup>*Instituto de Física de São Carlos, Universidade de São Paulo, 13560-970 São Carlos, SP, Brazil*

(Received 30 March 2011; published 20 July 2011)

Atomic clouds prepared in “timed Dicke” states, i.e. states where the phase of the oscillating atomic dipole moments linearly varies along one direction of space, are efficient sources of superradiant light emission [Scully *et al.*, *Phys. Rev. Lett.* **96**, 010501 (2006)]. Here, we show that, in contrast to previous assertions, timed Dicke states are *not* the states automatically generated by incident laser light. In reality, the atoms act back on the driving field because of the finite refraction of the cloud. This leads to nonuniform phase shifts, which, at higher optical densities, dramatically alter the cooperative scattering properties, as we show by explicit calculation of macroscopic observables, such as the radiation pressure force.

DOI: [10.1103/PhysRevA.84.013821](https://doi.org/10.1103/PhysRevA.84.013821)

PACS number(s): 42.50.Nn, 37.10.Vz, 42.25.Fx

### I. INTRODUCTION

The fact that ensembles of point-like scatterers respond collectively to incident radiation has been well-known since the seminal paper of Dicke [1]. The collective phenomenon, termed superradiance, has been the topic of several theoretical and experimental works. However, the question about the exact nature of the state generated by the radiation traveling through the ensemble has only been raised recently. Scully and coworkers [2] pointed out that the dipole moments of scatterers distributed along the incident beam’s optical axis are excited *in phase* with beam’s propagating phase front. The resulting “timed Dicke” state emits light predominantly into forward direction, provided the ensemble size is large compared to the radiation wavelength [3].

This simple picture, however, only holds at low optical densities. At high optical densities and spherically symmetric ensembles, the refraction index of the scattering medium delays the propagation of the pump beam and distorts its phase front. This distortion can have a significant impact on any macroscopic observable of the system, such as the angular distribution of the scattered radiation, the phase-front of the transmitted beam, or the force acting on the center-of-mass of the ensemble.

The aim of this paper is to calculate the correct state generated in an ensemble of two-level systems, e.g., an atomic cloud, by interaction with a weak laser beam and how this state cooperatively scatters the incident light. Cooperative scattering by many atoms has been studied extensively in the past, both classically and quantum-mechanically. Classically, scattering at extended objects is described as Mie scattering, showing resonances induced by the boundary conditions that the target imposes to the incident light field [4]. Quantum-mechanically, Dicke [1] has shown that when two-level atoms are confined inside a volume much smaller than a radiation wavelength, the emission can be superradiant or subradiant. How the classical and quantum pictures are linked has been demonstrated at the example of a sample of weakly excited atoms [5,6]. More precisely, when a single atom out of  $N$  is excited, the Dicke symmetric state of maximum cooperation radiates superradiantly, i.e., at a decay rate proportional to  $N$ . Cooperative effects related to the superradiant and directional

emission by an extended ensemble of atoms in a timed symmetric Dicke state have been observed in the radiation pressure force acting on a large cloud of atoms driven by a resonant radiation field. Depending on the detuning of the incident radiation frequency from atomic resonance, the radiation pressure force may be either drastically reduced due to both increased forward scattering and a reduced scattering cross section [3,7], or even enhanced if the cooperative Mie scattering dominates over superradiance [8].

In this paper, we revisit the scattering by  $N$  atoms driven by a constant uniform radiation field and emitting radiation into free space. Our description assumes several approximations: (1) weak excitation of the atomic ensemble (one atom out of  $N$  is excited); (2) Markov or “rapid transit” approximation [5] (photon time of flight through the cloud much shorter than atomic decay time); (3) atoms frozen (zero temperature) and motionless; (4) neglected dipole-dipole interactions and collisions; (5) neglected nonresonant interactions, i.e. nonresonant fluorescence, Van der Waals interactions, etc. Approximation (3) excludes several cooperative effects related to atomic recoil motion (e.g., collective atom recoil lasing [9,10] or matter wave superradiance [11,12]) and thus neglects stimulated scattering processes along preferential directions, as, for instance, end-fire modes in Bose-Einstein condensates [13] or optical cavity modes [14]. Neglecting atomic interactions [approximation (4)] is justified assuming atomic distances much larger than an optical wavelength. The interesting opposite regime (atoms closer than an optical wavelength) requires the solution of the atomic equations with an exponential interaction kernel [see Eq. (3)] and will be discussed in a future publication.

We here determine the stationary solution for a spherical Gaussian distribution, as well as relevant macroscopic quantities such as medium polarization, scattered radiation intensity, and radiation pressure force. Our solution is based on a solution of the eigenvalue problem in the smooth density approximation. For large size samples, a continuous spectrum limit allows us to obtain explicit analytical expressions for such quantities, expressed as a function of experimentally controllable parameters such as frequency and power of the driving field, optical thickness, and size of the atomic sample.

The paper is organized as follow: in Sec. II, the scattering problem is expressed in terms of multiparticle coupled differential equations. In Sec. III, the continuous density approximation is introduced and the solution for the atomic field is found in terms of the discrete eigenvalues of the interaction operator. Then, some macroscopic quantities of importance are calculated in Sec. IV. A continuous spectrum approximation for large atomic clouds performed in Sec. V appears to be particularly suitable to evaluate macroscopic quantities for arbitrarily large values of atomic density. Section VI revises the radiation pressure force obtained assuming a symmetric timed Dicke atomic state [3] and, comparing this state to the exact solution, we find that phase shifts induced by the atomic cloud's refractive index are at the origin of important corrections for the expectation values of macroscopic quantities. Finally, numerical results and conclusions are presented in Sec. VII.

## II. COOPERATIVE SCATTERING PROBLEM

A system of two-level ( $g$  and  $e$ ) atoms with resonant frequency  $\omega_a$  and position  $\mathbf{r}_j$ , driven by a uniform laser beam with electric field amplitude  $E_0$ , frequency  $\omega_0$ , and wave vector  $\mathbf{k}_0 = (\omega_0/c)\hat{\mathbf{e}}_z$ , is described by the interaction Hamiltonian:

$$H = \frac{\hbar\Omega_0}{2} \sum_{j=1}^N [\hat{\sigma}_j e^{i(\Delta_0 t - \mathbf{k}_0 \cdot \mathbf{r}_j)} + \text{H.c.}] + \hbar \sum_{j=1}^N \sum_{\mathbf{k}} g_{\mathbf{k}} (\hat{\sigma}_j e^{-i\omega_a t} + \hat{\sigma}_j^\dagger e^{i\omega_a t}) \times [\hat{a}_{\mathbf{k}}^\dagger e^{i(\omega_{\mathbf{k}} t - \mathbf{k} \cdot \mathbf{r}_j)} + \hat{a}_{\mathbf{k}} e^{-i(\omega_{\mathbf{k}} t - \mathbf{k} \cdot \mathbf{r}_j)}], \quad (1)$$

where  $\Omega_0 = dE_0/\hbar$  is the Rabi frequency of the incident laser field,  $\hat{\sigma}_j$  is the lowering operator for atom  $j$ ,  $\hat{a}_{\mathbf{k}}$  is the photon annihilation operator, and  $g_{\mathbf{k}} = (d^2\omega_{\mathbf{k}}/2\hbar\epsilon_0 V_{\text{ph}})^{1/2}$  is the single-photon Rabi frequency, where  $d$  is the electric-dipole transition matrix element and  $V_{\text{ph}}$  is the photon volume. A special case is when a single photon is present in the mode  $\mathbf{k}$ , as was extensively investigated in Refs. [2,15,16]. The total system (atoms+photons) is assumed to be in a state of the form [6]

$$|\Psi\rangle = \alpha(t)|g_1 \dots g_N\rangle|0\rangle_{\mathbf{k}} + e^{-i\Delta_0 t} \sum_{j=1}^N \beta_j(t)|g_1 \dots e_j \dots g_N\rangle \times |0\rangle_{\mathbf{k}} + \sum_{\mathbf{k}} \gamma_{\mathbf{k}}(t)|g_1 \dots g_N\rangle|1\rangle_{\mathbf{k}} + \sum_{m,n=1}^N \epsilon_{m<n,\mathbf{k}}(t)|g_1 \dots e_m \dots e_n \dots g_N\rangle|1\rangle_{\mathbf{k}}, \quad (2)$$

where  $\Delta_0 = \omega_0 - \omega_a$ . The first term corresponds to the initial ground state without photons; the sum in the second term is the state where a single atom has been excited by the classical field. The third term corresponds to the atom returned to the ground state having emitted a photon in the mode  $\mathbf{k}$ , whereas the last one corresponds to the presence of two excited atoms and one virtual photon with “negative” energy. It is due to the counter-rotating terms in the Hamiltonian Eq. (1) and disappears when the rotating wave approximation (RWA) is

made. In the linear regime (i.e.,  $\alpha \approx 1$ ) and in the Markov approximation (valid if the decay time is larger than the photon time-of-flight through the atomic cloud), the problem reduces to the following differential equation [19]:

$$\dot{\beta}_j = \left(i\Delta_0 - \frac{\Gamma}{2}\right) \beta_j - i\frac{\Omega_0}{2} e^{i\mathbf{k}_0 \cdot \mathbf{r}_j} + i\frac{\Gamma}{2} \sum_{m \neq j} \frac{\exp(i k_0 |\mathbf{r}_j - \mathbf{r}_m|)}{k_0 |\mathbf{r}_j - \mathbf{r}_m|} \beta_m, \quad (3)$$

where  $\Gamma = V_{\text{ph}} g_{\mathbf{k}}^2 k_0^2 / \pi c$  is the single-atom *spontaneous* decay rate. The kernel in the last term of Eq. (3) has a real component,  $-(\Gamma/2) \sum_{m \neq j} [\sin(\rho_{jm})/\rho_{jm}]$  (where  $\rho_{jm} = k_0 |\mathbf{r}_j - \mathbf{r}_m|$ ), describing the *collective* atomic decay, and an imaginary component,  $i(\Gamma/2) \sum_{m \neq j} [\cos(\rho_{jm})/\rho_{jm}]$ , describing the collective Lamb shift due to short-range interaction between atoms, induced by the electromagnetic field [19–21]. The latter becomes significant when the number of atoms in a cubic optical wavelength,  $n\lambda^3$ , is larger than unity, in which case the contribution from the virtual processes described by the counter-rotating terms in the Hamiltonian becomes relevant. Hence, for a sufficiently dilute system, such that  $N \ll \sigma^3$ , where  $\sigma = k_0 \sigma_R$  and  $\sigma_R$  is the cloud size, the collective phase shift arising from the imaginary part of the kernel in Eq. (3) can be disregarded [22] and the scattering problem reduces to

$$\dot{\beta}_j = \left(i\Delta_0 - \frac{\Gamma}{2}\right) \beta_j - i\frac{\Omega_0}{2} e^{i\mathbf{k}_0 \cdot \mathbf{r}_j} - \frac{\Gamma}{2} \sum_{m \neq j} \frac{\sin(k_0 |\mathbf{r}_j - \mathbf{r}_m|)}{k_0 |\mathbf{r}_j - \mathbf{r}_m|} \beta_m, \quad (4)$$

with initial condition  $\beta_j(0) = 0$ , for  $j = 1, \dots, N$ . Notice that Eq. (3) deduced in the quantum mechanical description may be also obtained classically when the two-level atoms are treated as weakly excited classical harmonic oscillators [5,6]. For this reason, the solution of Eq. (3) [or of the approximated version, Eq. (4)] has a wider interest for the general problem of collective radiation scattering.

As for the radiation field operator  $\hat{a}_{\mathbf{k}}$ , it evolves according the Heisenberg equation,

$$\frac{d\hat{a}_{\mathbf{k}}}{dt} = \frac{1}{i\hbar} [\hat{a}_{\mathbf{k}}, \hat{H}] = -i g_{\mathbf{k}} e^{i(\omega_{\mathbf{k}} - \omega_a)t} \sum_{m=1}^N \hat{\sigma}_m e^{-i\mathbf{k} \cdot \mathbf{r}_m}, \quad (5)$$

where the fast oscillating term proportional to  $\exp[i(\omega_{\mathbf{k}} + \omega_a)t]$  has been neglected.

## III. CONTINUOUS DENSITY APPROXIMATION

In light scattering experiments, disorder (or granularity) plays a role when the number of atoms projected onto a cross section perpendicular to the incident beam is small enough so that a light mode focused down to the diffraction limit (that is  $\sim \lambda^2$ ) would be able to resolve and count the atoms. In other words, the stochastic fluctuations induced by the random positions of the atoms can be neglected when the total number of atoms  $N$  is larger than the number of modes  $\sim \sigma^2$  that fit into the cloud's cross section, i.e., when the optical density is  $b_0 = 3N/\sigma^2 \gg 1$ . Under this hypothesis, the particles can be

described by a smooth density  $n(\mathbf{r})$  and their probability to be excited by a field  $\beta(\mathbf{r}, t)$ , so that Eq. (4) turns into

$$\frac{\partial}{\partial t} \beta(\mathbf{r}, t) = \left( i\Delta_0 - \frac{\Gamma}{2} \right) \beta(\mathbf{r}, t) - i \frac{\Omega_0}{2} e^{i\mathbf{k}_0 \cdot \mathbf{r}} - \frac{\Gamma}{2} \int d\mathbf{r}' n(\mathbf{r}') \frac{\sin(k_0|\mathbf{r} - \mathbf{r}'|)}{k_0|\mathbf{r} - \mathbf{r}'|} \beta(\mathbf{r}', t). \quad (6)$$

In what follows we will consider only spherically symmetric distributions  $n(r)$ . Because of the linearity of Eq. (6), it is convenient to introduce an eigenbasis of the coupling operator. The functions  $j_n(r)Y_{nm}(\theta, \phi)$ , with  $j_n$ s the spherical Bessel functions and  $Y_{nm}(\theta, \phi)$ s the spherical harmonics, appear as a natural choice considering the following identity:

$$\frac{\sin(k_0|\mathbf{r} - \mathbf{r}'|)}{k_0|\mathbf{r} - \mathbf{r}'|} = 4\pi \sum_{n=0}^{\infty} \sum_{m=-n}^n j_n(k_0r) Y_{nm}^*(\theta, \phi) \times Y_{nm}(\theta', \phi') j_n(k_0r'). \quad (7)$$

In particular, the choice of the spherical harmonics guarantees the orthogonality of the basis, since

$$\int_0^{2\pi} d\phi \int_0^\pi d\theta \sin\theta Y_{nm}^*(\theta, \phi) Y_{n'm'}(\theta, \phi) = \delta_{nn'} \delta_{mm'}. \quad (8)$$

Therefore, assuming the following decomposition for the field,

$$\beta(\mathbf{r}, t) = \sum_{n=0}^{\infty} \sum_{m=-n}^n \alpha_{nm}(t) j_n(k_0r) Y_{nm}(\theta, \phi), \quad (9)$$

the projection of Eq. (6) along the eigenmodes leads to

$$\left[ \dot{\alpha}_{nm} - i\Delta_0 \alpha_{nm} + \frac{\Gamma}{2} (1 + \lambda_n) \alpha_{n,m} \right] j_n(k_0r) = -\frac{i}{2} \Omega_{nm}, \quad (10)$$

where  $\lambda_n$  are the eigenvalues associated to modes  $n$ ,

$$\lambda_n = 4\pi \int_0^\infty r^2 n(r) j_n^2(k_0r) dr, \quad (11)$$

whereas  $\Omega_{nm}$  corresponds to the projection of the incident wave on mode  $(n, m)$ ,

$$\begin{aligned} \Omega_{nm} &= \Omega_0 \int_0^{2\pi} d\phi \int_0^\pi d\theta \sin\theta Y_{nm}^*(\theta, \phi) e^{i\mathbf{k}_0 \cdot \mathbf{r} \cos\theta} \\ &= 2\Omega_0 \delta_{m0} \sqrt{\pi(2n+1)} i^n j_n(k_0r). \end{aligned} \quad (12)$$

Assuming the cloud is initially unexcited, i.e.,  $\alpha_{nm}(0) = 0$ , only spherically symmetric components with  $m = 0$  will grow so that, defining  $\alpha_n(t) \equiv \alpha_{n0}(t)$ , Eq. (10) reduces to

$$\dot{\alpha}_n - \left[ i\Delta_0 - \frac{\Gamma}{2} (1 + \lambda_n) \right] \alpha_n = -i^{n+1} \sqrt{\pi(2n+1)} \Omega_0. \quad (13)$$

Equation (13) straightforwardly integrates and, inserted in Eq. (9), leads to the following expression for the excitation field

$$\begin{aligned} \beta(r, \theta, t) &= \frac{\Omega_0}{\Gamma} \sum_{n=0}^{\infty} \frac{i^n (2n+1) j_n(k_0r) P_n(\cos\theta)}{2\delta + i(1 + \lambda_n)} \\ &\times [1 - e^{i\Delta_0 t} e^{-(\Gamma/2)(1 + \lambda_n)t}], \end{aligned} \quad (14)$$

where the scaled detuning  $\delta = \Delta_0/\Gamma$  was introduced. Hence, each mode  $n$  relaxes toward the steady-state with a characteristic time  $\tau_n = 1/\Gamma(1 + \lambda_n)$ : the first modes relax very quickly since  $\lambda_n$  is proportional to  $N$ , yet for the highest modes,  $\tau_n \sim \Gamma^{-1}$ , even if their macroscopic contribution is usually small. Eventually, for times much longer than the single-atom decay time  $\Gamma^{-1}$ , the field tends toward a stationary state fully characterized by the spectrum

$$\beta_s(r, \theta) = \frac{\Omega_0}{\Gamma} \sum_{n=0}^{\infty} \frac{i^n (2n+1)}{2\delta + i(1 + \lambda_n)} j_n(k_0r) P_n(\cos\theta). \quad (15)$$

Notice that the set of eigenvalues in Eq. (11) is complete since from the identity  $\sum_{n \geq 0} (2n+1) j_n^2(z) = 1$ , it follows that

$$\sum_{n=0}^{\infty} (2n+1) \lambda_n = 4\pi \int_0^\infty r^2 n(r) dr = N, \quad (16)$$

which corresponds to the trace of the coupling operator.

#### IV. MACROSCOPIC QUANTITIES

The description of the field  $\beta_s(r, \theta)$  in terms of spectrum also provides expressions for any macroscopic quantities, the most relevant of which are calculated here below. These formulae will be specialized to Gaussian clouds in the subsequent section.

##### A. Average amplitude and probability of excitation

The average ‘‘phased’’ probability of the timed Dicke state [19] and the excitation probability are, respectively,

$$\langle \beta_s e^{-i\mathbf{k}_0 \cdot \mathbf{r}} \rangle = \frac{2\pi}{N} \int_0^\pi d\theta \sin\theta \int_0^\infty dr r^2 n(r) \beta_s(r, \theta) e^{-ik_0r \cos\theta} \quad (17)$$

$$\langle |\beta_s|^2 \rangle = \frac{2\pi}{N} \int_0^\pi d\theta \sin\theta \int_0^\infty dr r^2 n(r) |\beta_s(r, \theta)|^2. \quad (18)$$

Inserting Eq. (15) and using the identities

$$\int_{-1}^1 dx P_n(x) e^{i\alpha x} = 2i^n j_n(\alpha), \quad (19)$$

$$\int_{-1}^1 dx P_m(x) P_n(x) = \frac{2}{2n+1} \delta_{mn},$$

we obtain

$$\langle \beta_s e^{-i\mathbf{k}_0 \cdot \mathbf{r}} \rangle = \frac{\Omega_0}{\Gamma N} \sum_{n=0}^{\infty} \frac{(2n+1) \lambda_n}{2\delta + i(1 + \lambda_n)} \quad (20)$$

$$\langle |\beta_s|^2 \rangle = \frac{\Omega_0^2}{\Gamma^2 N} \sum_{n=0}^{\infty} \frac{(2n+1) \lambda_n}{4\delta^2 + (1 + \lambda_n)^2}. \quad (21)$$

##### B. Scattered field

The electric field radiated by the excited atoms reads, in the smooth density limit (see Appendix A),

$$\mathcal{E}_S(r, \theta, \phi, t) = -\frac{dk_0^2}{4\pi \epsilon_0 r} e^{ik_0(r-ct)} \int d\mathbf{r}' n(\mathbf{r}') \beta(\mathbf{r}', t) e^{-i\mathbf{k}_s \cdot \mathbf{r}'}. \quad (22)$$

Using the stationary solution of Eq. (15) for a spherically symmetric distribution and using the integral

$$\int_0^\pi d\theta' \sin\theta' P_n(\cos\theta') J_0(k_0 r' \sin\theta \sin\theta') e^{-ik_0 r' \cos\theta \cos\theta'} = 2i^{-n} j_n(k_0 r') P_n(\cos\theta), \quad (23)$$

we obtain

$$\mathcal{E}_S(r, \theta) = - \left( \frac{E_0}{4\pi k_0 r} \right) e^{ik_0(r-ct)} \sum_{n=0}^{\infty} \frac{(2n+1)\lambda_n}{2\delta+i(1+\lambda_n)} P_n(\cos\theta), \quad (24)$$

where we used the relation  $\Gamma = d^2 k_0^3 / (2\pi \hbar \epsilon_0)$ . In the forward direction ( $\theta = 0$ ), the scattered field is proportional to the ‘‘phased’’ probability amplitude (20). Equation (24) provides the angular distribution of the scattered radiation field. We can also calculate the scattered intensity as

$$\begin{aligned} I_S(r, \theta, \phi) &= c\epsilon_0 \langle \hat{E}_S^\dagger \hat{E}_S \rangle \\ &= c\epsilon_0 \left( \frac{dk_0^2}{4\pi\epsilon_0 r} \right)^2 \left[ \sum_{j=1}^N |\beta_j|^2 + \sum_{j \neq m} \beta_m^* \beta_j e^{-i\mathbf{k}_j \cdot (\mathbf{r}_j - \mathbf{r}_m)} \right]. \end{aligned} \quad (25)$$

Passing to the continuous limit and using Eqs. (21), (22), and (24), we obtain

$$\begin{aligned} I_S(r, \theta) &= \frac{I_0}{(4\pi k_0 r)^2} \left[ \sum_{n=0}^{\infty} \frac{(2n+1)\lambda_n}{4\delta^2 + (1+\lambda_n)^2} \right. \\ &\quad \left. + \left| \sum_{n=0}^{\infty} \frac{(2n+1)\lambda_n}{2\delta+i(1+\lambda_n)} P_n(\cos\theta) \right|^2 \right], \end{aligned} \quad (26)$$

where  $I_0 = c\epsilon_0 E_0^2$ . The scattered intensity is the sum of the incoherent contribution, proportional to  $N$  [since  $\lambda_n \propto N$ , see Eq. (11)] and isotropic, and the superradiant contribution, proportional to  $N^2$  and directed (for extended clouds) mainly in the forward direction. Integrating over the solid angle, the total scattered power is

$$\begin{aligned} P_S &= 2\pi r^2 \int_0^\pi d\theta \sin\theta I_S(r, \theta) \\ &= \left( \frac{I_0}{4\pi k_0^2} \right) \sum_{n=0}^{\infty} \frac{(2n+1)\lambda_n(1+\lambda_n)}{4\delta^2 + (1+\lambda_n)^2}, \end{aligned} \quad (27)$$

where we used the second of the identities of Eq. (19).

### C. Radiation pressure force

The radiation force operator acting on the  $j$ th atom is calculated from Eq. (1) as  $\hat{\mathbf{F}}_j = -\nabla_{\mathbf{r}_j} \hat{H} = \hat{\mathbf{F}}_{aj} + \hat{\mathbf{F}}_{ej}$ , where [3]

$$\hat{\mathbf{F}}_{aj} = i\hbar \mathbf{k}_0 \frac{\Omega_0}{2} \{ \hat{\sigma}_j e^{i(\Delta_0 t - \mathbf{k}_0 \cdot \mathbf{r}_j)} - \text{H.c.} \} \quad (28)$$

$$\hat{\mathbf{F}}_{ej} = i\hbar \sum_{\mathbf{k}} \mathbf{k} g_{\mathbf{k}} \{ \hat{a}_{\mathbf{k}}^\dagger \hat{\sigma}_j e^{i(\omega_{\mathbf{k}} - \omega_a)t - i\mathbf{k} \cdot \mathbf{r}_j} - \hat{\sigma}_j^\dagger \hat{a}_{\mathbf{k}} e^{-i(\omega_{\mathbf{k}} - \omega_a)t + i\mathbf{k} \cdot \mathbf{r}_j} \} \quad (29)$$

are the forces due, respectively, to the absorption and emission processes. In Eq. (29), we have neglected the counter-rotating terms proportional to  $\exp[\pm i(\omega_{\mathbf{k}} + \omega_a)t]$ . We are here interested in the average radiation force  $\hat{\mathbf{F}} = (1/N) \sum_j \hat{\mathbf{F}}_j$ , which stands for the force acting on the center-of-mass of the atomic cloud along the direction of the incident field,  $\mathbf{k}_0 = k_0 \hat{\mathbf{e}}_z$ . This average force is relatively easy to measure by time-of-flight techniques in cold atomic clouds released, for instance, from magneto-optical traps (MOTs) and has recently revealed cooperative effects in the scattering by extended atomic samples [7,8]. It may provide a convenient measurement (aside from the scattered radiation) of the effects that cooperative scattering imprints on the atoms. The average absorption force along the  $z$ -axis, resulting from the recoil received upon absorption of a photon from the incident laser, is

$$\hat{F}_a = \frac{i}{2N} \hbar k_0 \Omega_0 \sum_{j=1}^N [\hat{\sigma}_j e^{i\Delta_0 t - i\mathbf{k}_0 \cdot \mathbf{r}_j} - \text{H.c.}]. \quad (30)$$

The second contribution  $\hat{\mathbf{F}}_e = (1/N) \sum_j \hat{\mathbf{F}}_{ej}$  results from the emission of a photon into any direction  $\mathbf{k}$ . Inserting  $\hat{a}_{\mathbf{k}}$  from Eq. (5) into Eq. (29) and approximating the sum over the modes  $\mathbf{k}$  by an integral, it is possible to obtain, in a way similar as done for the radiation field operator  $\hat{E}_S$  of Eq. (A5), the following expression for the average emission force along the  $z$ -axis [3]:

$$\begin{aligned} \hat{F}_e &= -\frac{\hbar k_0 \Gamma}{8\pi N} \int_0^{2\pi} d\phi \int_0^\pi d\theta \sin\theta \cos\theta \\ &\quad \times \sum_{j,m=1}^N [e^{-i\mathbf{k} \cdot (\mathbf{r}_j - \mathbf{r}_m)} \hat{\sigma}_m^\dagger \hat{\sigma}_j + \text{H.c.}]. \end{aligned} \quad (31)$$

Evaluating their expectation values on the state of Eq. (2) (neglecting virtual photon contributions), the emission force in the discrete model is

$$\begin{aligned} \langle F_e \rangle &= -\frac{\hbar k_0 \Gamma}{8\pi N} \int_0^{2\pi} d\phi \int_0^\pi d\theta \sin\theta \cos\theta \\ &\quad \times \sum_{j,m=1}^N [\beta_j \beta_m^* e^{-i\mathbf{k} \cdot (\mathbf{r}_j - \mathbf{r}_m)} + \text{c.c.}] \\ &= i \frac{\hbar k_0 \Gamma}{2N} \sum_{j,m=1}^N \frac{(z_j - z_m)}{|\mathbf{r}_j - \mathbf{r}_m|} j_1(k_0 |\mathbf{r}_j - \mathbf{r}_m|) (\beta_j \beta_m^* - \text{c.c.}), \end{aligned} \quad (32)$$

where we used the identity (B1) and  $j_1(z)$  is the first-order spherical Bessel function. Then, passing to the continuous distribution limit, Eqs. (30) and (31) are approximated by

$$\langle \hat{F}_a \rangle = -\hbar k_0 \Omega_0 \text{Im} \langle \beta e^{-i\mathbf{k}_0 \cdot \mathbf{r}} \rangle \quad (33)$$

$$\begin{aligned} \langle \hat{F}_e \rangle &= -\hbar k_0 \frac{\Gamma}{8\pi N} \int_0^{2\pi} d\phi \int_0^\pi d\theta \sin\theta \cos\theta \int d\mathbf{r} n(r) \\ &\quad \times \int d\mathbf{r}' n(r') [\beta(\mathbf{r}) \beta^*(\mathbf{r}') e^{-i\mathbf{k} \cdot (\mathbf{r} - \mathbf{r}')} + \text{c.c.}]. \end{aligned} \quad (34)$$

The absorption stationary force is readily obtained from Eq. (20),

$$\langle \hat{F}_a \rangle = \hbar k_0 \frac{\Omega_0^2}{\Gamma N} \sum_{n=0}^{\infty} \frac{(2n+1)\lambda_n(1+\lambda_n)}{4\delta^2 + (1+\lambda_n)^2}, \quad (35)$$

whereas a longer calculation, reported in Appendix B, yields the emission stationary force,

$$\langle F_e \rangle = -\hbar k_0 \frac{2\Omega_0^2}{\Gamma N} \sum_{n=0}^{\infty} \frac{(n+1)\lambda_n\lambda_{n+1}[4\delta^2 + (1+\lambda_n)(1+\lambda_{n+1})]}{[4\delta^2 + (1+\lambda_n)^2][4\delta^2 + (1+\lambda_{n+1})^2]}. \quad (36)$$

As expected, the absorption force pushes the atomic cloud in the direction of the driving field, whereas the emission force is oppositely directed and is proportional to  $N$ . Both forces depend on  $N$  also through the collective decay rate  $\Gamma(1+\lambda_n)$ . We observe that the absorption force of Eq. (35) is linked to the scattered power of Eq. (27) by the relation

$$N\langle \hat{F}_a \rangle = 4\pi \left( \frac{P_S}{c} \right), \quad (37)$$

i.e., the absorption force is proportional to the scattered power per atom,  $P_S/N$ .

Figure 1 compares the (a) absorption, (b) emission, and (c) total forces vs.  $N$  for  $\delta = 10$  and a Gaussian density profile with  $\sigma = 8$  (where  $\sigma = k_0\sigma_R$ ), calculated using the series (35) and (36) (circles) and  $N$ -body simulations [see Eq. (4)] (dots). The eigenvalues  $\lambda_n$  for the Gaussian density profile are given by Eq. (38). The forces are reported as a ratio between the cooperative force and the single-atom force,  $F_1 = \hbar k_0\Gamma\Omega_0^2/(4\Delta_0^2 + \Gamma^2)$ . The error bars correspond to the standard deviation of the observables over eight realizations. Figure 1(d) shows the total force vs.  $N$  for a different choice of parameters,  $\sigma = 5$  and  $\delta = 200$ , for which the force exhibits a maximum as a function of  $N$  [8]. We observe a good agreement between the analytical solution of Eq. (35) and the  $N$ -body simulations at large  $N$ , when effects due to the discreteness of the system become negligible.

We recall that our expressions have been obtained in the continuous density approximation, i.e., assuming a sample with large optical thickness, i.e.,  $N \gg \sigma^2$ , but sufficiently dilute to neglect the collective Lamb shift, i.e., with a small number of atoms in a cubic optical wavelength volume,  $N \ll \sigma^3$ . These two conditions imply that the cloud size should be much larger than the optical wavelength,  $\sigma \gg 1$ . Nevertheless, our results remain valid also in the limit  $n(r) \rightarrow 0$ , where, in particular, the standard radiation pressure force,  $F_1$ , is recovered. However, at low densities, fluctuations will strongly affect individual measurements of the radiation pressure force,

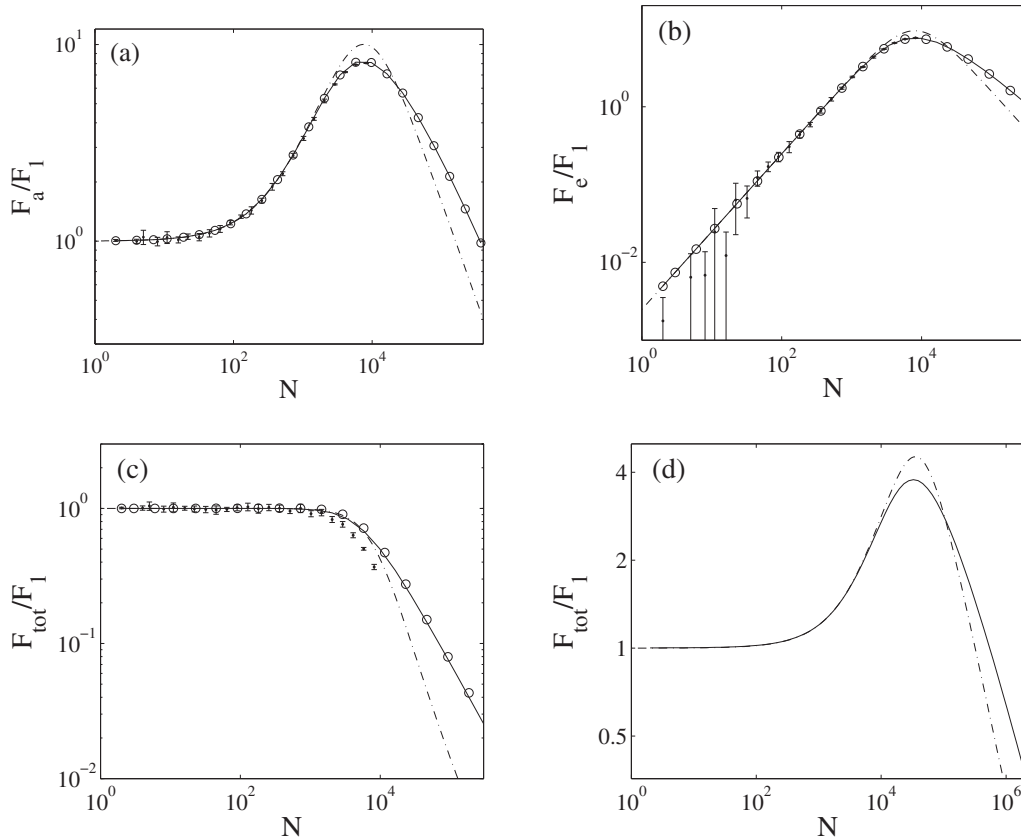


FIG. 1. (a) Absorption, (b) emission, and (c) total forces vs.  $N$  for  $\delta = 10$  and a Gaussian cloud with  $\sigma = 8$ . (d) Total force for  $\sigma = 5$  and  $\delta = 200$ . Forces are relative to the single-atom force  $F_1$ . The plain curves refer to the series (35), (36), and their sum; the circles to the analytical expressions (46), (36), and their sum; the dots to  $N$ -body simulations [see Eq. (4)] and the dash-dotted lines to the STD state. The error bars correspond to the standard deviation of the observables over eight realizations.

and in this regime our expressions represent only the average expectation values.

### V. LARGE GAUSSIAN CLOUDS

Large clouds ( $\sigma \gg 1$ ) behaves fundamentally differently from small clouds ( $\sigma \lesssim 1$ ), as can be deduced from their spectrum. Let us, for example, consider the case of Gaussian clouds, with density  $n(r) = [N/(2\pi)^{3/2}\sigma_R^3] \exp(-r^2/2\sigma_R^2)$ . The spectrum then reads

$$\begin{aligned} \lambda_n &= N \sqrt{\frac{2}{\pi}} \int_0^\infty \rho^2 e^{-\rho^2/2} j_n^2(\sigma\rho) d\rho \\ &= N \sqrt{\frac{\pi}{2\sigma^2}} e^{-\sigma^2} I_{n+1/2}(\sigma^2), \end{aligned} \quad (38)$$

where  $\sigma = k_0\sigma_R$  is the scaled size of the cloud, and  $I_n(x)$  the  $n$ th modified Bessel function. Recently the spectrum  $\lambda_n$  for an uniform spherical cloud has been calculated by Svidzinsky *et al.* [6,16], also for the exponential kernel of Eq. (3). However, a Gaussian distribution is certainly more realistic for experiments with cold dense atomic ensembles. Generally, the spectrum of small clouds ( $\sigma \leq 1$ ) is composed of a few significant eigen modes, whereas for  $\sigma$  large, all the eigenmodes for  $n < \sigma$  are significant and the spectrum can be treated as a continuum. In particular, in the latter case the  $\lambda_n$  can be approximated, for  $n < \sigma$ , by  $\lambda_n \sim (N/2\sigma^2) \exp[-(n+1/2)^2/2\sigma^2]$  (see, e.g., Ref. [17]). Switching to a continuous treatment of the spectrum, we define  $\eta = n + 1/2$  and get

$$\lambda_\eta = \frac{N}{2\sigma^2} e^{-\eta^2/(2\sigma^2)}. \quad (39)$$

$$\sum_{n=0}^{\infty} (2n+1) \rightarrow 2 \int_0^{\infty} \eta d\eta. \quad (40)$$

Remark that using these definitions, the completeness condition Eq. (16) is still preserved. The continuous spectrum limit allows for the evaluation of the sums in Eqs. (20) and (21) as continuous integrals

$$\begin{aligned} \langle \beta_s e^{-i\mathbf{k}_0 \cdot \mathbf{r}} \rangle &= \frac{2\Omega_0}{\Gamma N} \int_0^\infty \frac{\lambda_\eta \eta d\eta}{2\delta + i(1 + \lambda_\eta)} \\ &= \frac{\Omega_0}{\Gamma} \frac{6}{b_0} \int_0^{b_0/6} \frac{dx}{2\delta + i(1+x)} \end{aligned} \quad (41)$$

$$\langle \hat{F}_e \rangle = -\hbar k_0 \frac{\Omega_0^2 b_0}{6\Gamma} e^{-1/(4\sigma^2)} \int_{1/\sigma}^\infty dy \frac{y e^{-y^2} \{4\delta^2 + [1 + (b_0/6)e^{-(y+1/2\sigma)^2/2}][1 + (b_0/6)e^{-(y-1/2\sigma)^2/2}]\}}{\{4\delta^2 + [1 + (b_0/6)e^{-(y+1/2\sigma)^2/2}]^2\} \{4\delta^2 + [1 + (b_0/6)e^{-(y-1/2\sigma)^2/2}]^2\}}, \quad (47)$$

where we have set  $y = (\eta + 1)/\sigma$ . As can be observed in Fig. 1, the continuous-spectrum approximation gives excellent results compared to the full series Eqs. (35) and (36). In the limit  $\sigma \rightarrow \infty$  and finite  $b_0$ , Eq. (47) would lead to

$$\langle \hat{F}_e \rangle \approx -\langle \hat{F}_a \rangle + \hbar k_0 \Gamma \langle |\beta_s|^2 \rangle, \quad (48)$$

which has a transparent interpretation: for a very large cloud, the atoms scatter radiation to forward direction and the recoil

$$\begin{aligned} \langle |\beta_s|^2 \rangle &= \frac{2\Omega_0^2}{\Gamma^2 N} \int_0^\infty \frac{\lambda_\eta \eta d\eta}{4\delta^2 + (1 + \lambda_\eta)^2} \\ &= \left( \frac{\Omega_0}{\Gamma} \right)^2 \frac{6}{b_0} \int_0^{b_0/6} \frac{dx}{4\delta^2 + (1+x)^2}, \end{aligned} \quad (42)$$

where we have set  $x = (b_0/6) \exp(-\eta^2/2\sigma^2)$ , with  $b_0 = 3N/\sigma^2$  the optical thickness. The above expressions integrate as

$$\begin{aligned} \langle \beta_s e^{-i\mathbf{k}_0 \cdot \mathbf{r}} \rangle &= \left( \frac{\Omega_0}{\Gamma} \right) \frac{3}{b_0} \left\{ 2 \arctan \left[ \frac{b_0}{3} \frac{\delta}{1 + 4\delta^2 + b_0/6} \right] \right. \\ &\quad \left. - i \ln \left[ 1 + \frac{b_0}{3} \frac{1 + b_0/12}{1 + 4\delta^2} \right] \right\} \end{aligned} \quad (43)$$

$$\langle |\beta_s|^2 \rangle = \left( \frac{\Omega_0}{\Gamma} \right)^2 \frac{3}{\delta b_0} \arctan \left[ \frac{\delta b_0/3}{1 + 4\delta^2 + b_0/6} \right]. \quad (44)$$

These formulas highlight the prominent role of the parameters  $b_0$  and  $\delta$  in the high-density limit. In a similar way, we calculate the total scattered power as

$$\begin{aligned} P_S &= \frac{I_0 N}{4\pi k_0^2} \int_0^1 dx \frac{1 + (b_0/6)x}{4\delta^2 + [1 + (b_0/6)x]^2} \\ &= \frac{I_0 \sigma_R^2}{4\pi} \ln \left[ 1 + \frac{b_0}{3} \frac{1 + b_0/12}{1 + 4\delta^2} \right]. \end{aligned} \quad (45)$$

As expected, for small optical thickness ( $b_0 \ll 1$ ), the scattered power is incoherent,  $P_S \approx [I_0 N / (4\pi k_0^2)] / (4\delta^2 + 1)$ . However, for large optical thickness it shows a logarithmic dependence on  $N$ . The superradiant character of the radiation is visible only observing the scattered intensity in the forward direction [see the second term of Eq. (26)] but not in the total scattered power.

The absorption force is deduced from Eqs. (33) and (43) as

$$\langle \hat{F}_a \rangle = \hbar k_0 \frac{3\Omega_0^2}{b_0 \Gamma} \ln \left[ 1 + \frac{b_0}{3} \frac{1 + b_0/12}{1 + 4\delta^2} \right]. \quad (46)$$

The emission force can be written, in the continuous spectrum approximation in the integral form

received by the atoms upon emission cancels out with the recoil received by absorbing a photon from the driving field. The net force remaining after the subtraction is the noncollective contribution to the emission. The net force is equal to the photon momentum  $\hbar k_0$  times the emission rate  $\Gamma \langle |\beta_s|^2 \rangle$ . This emission rate depends indirectly on  $N$  and  $\sigma$  through the enhanced superradiant decay,  $\Gamma(N/4\sigma^2)$ , which decreases the emission rate when the optical thickness increases. A more accurate expression of the emission force valid for large but

finite cloud size would require the exact evaluation of the integral in Eq. (47).

## VI. SYMMETRIC TIMED DICKE STATE

A particular ansatz used by Scully and coworkers [2,6,16] is the symmetric timed Dicke (STD) state, given by

$$\beta(\mathbf{r}, t) = \beta_{TD}(t)e^{i\mathbf{k}_0 \cdot \mathbf{r}}. \quad (49)$$

After integration over space of Eq. (6), one obtains the following evolution equation:

$$\frac{d\beta_{TD}(t)}{dt} = \left[ i\Delta_0 - \frac{\Gamma}{2}(1 + Ns_\infty) \right] \beta_{TD}(t) - i\frac{\Omega_0}{2}, \quad (50)$$

where  $s_\infty$  is the integrated structure factor of the cloud defined as

$$\begin{aligned} s_\infty &= \frac{1}{N^2} \int n(\mathbf{r}) d\mathbf{r} \int d\mathbf{r}' n(\mathbf{r}') \frac{\sin(k_0|\mathbf{r} - \mathbf{r}'|)}{k_0|\mathbf{r} - \mathbf{r}'|} e^{-i\mathbf{k}_0 \cdot (\mathbf{r} - \mathbf{r}')} \\ &= \frac{1}{4\pi} \int_0^{2\pi} d\phi \int_0^\pi d\theta \sin\theta | \langle e^{i(\mathbf{k}_0 - \mathbf{k}) \cdot \mathbf{r}} \rangle |^2. \end{aligned} \quad (51)$$

This ansatz is of particular interest, since it allows to evidence, e.g., the superradiant nature of the decay when the pump is turned off [19]. As for its steady-state, it reads [3,7]

$$\beta_{TD} = \frac{\Omega_0}{\Gamma} \frac{1}{2\delta + i(1 + Ns_\infty)}, \quad (52)$$

and for a large cloud with Gaussian distribution, since  $s_\infty \approx 1/4\sigma^2$ , we get

$$\beta_{TD} = \frac{\Omega_0}{\Gamma} \frac{1}{2\delta + i(1 + b_0/12)}. \quad (53)$$

Thus, the STD solution of Eq. (53) approximates the exact result of Eq. (44) only for  $b_0 \ll 12$ ,

$$|\beta_{TD}|^2 \approx \left( \frac{\Omega_0}{\Gamma} \right)^2 \frac{1}{4\delta^2 + (1 + b_0/6)}. \quad (54)$$

Figure 2 shows the average excitation probability  $\langle |\beta_s|^2 \rangle$  (left) and its variance,  $\sigma_\beta^2 = \langle |\beta_s|^2 \rangle - |\langle \beta_s e^{-i\mathbf{k}_0 \cdot \mathbf{r}} \rangle|^2$  vs.  $N$  for

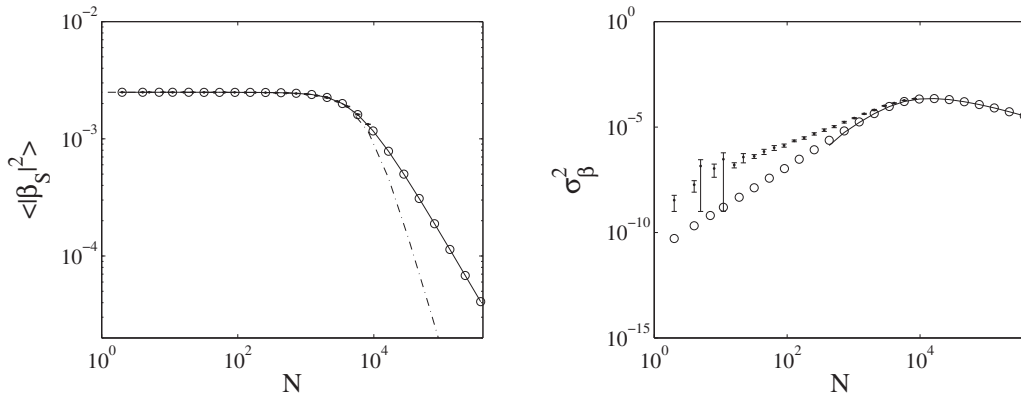


FIG. 2. Average excitation probability  $\langle |\beta_s|^2 \rangle$  (left) and variance  $\sigma_\beta^2 = \langle |\beta_s|^2 \rangle - |\langle \beta_s e^{-i\mathbf{k}_0 \cdot \mathbf{r}} \rangle|^2$  (right) vs.  $N$ . The plain curves refer to the analytical Eqs. (43) and (44), the circles to series Eqs. (20) and (21), the dots to  $N$ -body simulations (see Eq. (4)), and the dash-dotted lines to the STD state. The error bars correspond to the standard deviation of the observables over eight realizations. Note that for the STD state,  $\sigma_\beta = 0$ ; for too small  $N$ , the approximation Eqs. (43) and (44) provide inconsistent results, that is negative  $\sigma_\beta$ . Simulations realized for  $\sigma = 10$  and  $\delta = 10$ .

$\sigma = 10$  and  $\delta = 10$ . The plain curves refer to the analytical Eqs. (43) and (44), the circles to series Eqs. (20) and (21), the dots to  $N$ -body simulations (see Eq. (4)), and the dash-dotted lines to the STD state Eq. (49). The error bars correspond to the standard deviation of the observables over different realizations. Note that for the STD state,  $\sigma_\beta = 0$ ; for too small  $N$ , the approximation Eqs. (43) and (44) provide inconsistent results, that is negative  $\sigma_\beta^2$ . We observe excellent agreement between the series and the analytical solutions, and a consistent reduction of the excitation probability decrease vs.  $N$  with respect to the TDS prediction (dashed line in Fig. 2, left). Also, the fluctuations obtained from the  $N$ -body simulations converge for large values of  $N$  toward the results obtained in the continuous density approximation (Fig. 2, left), showing the presence of a shot-noise contribution for small  $N$ .

The radiation force for the STD ansatz Eq. (49) is [3,7,8]

$$\langle \hat{F} \rangle = \langle \hat{F}_a \rangle + \langle \hat{F}_e \rangle = \hbar k_0 [-\Omega_0 \text{Im}(\beta_{TD}) - \Gamma |\beta_{TD}|^2 N f_\infty], \quad (55)$$

where

$$f_\infty = \frac{1}{4\pi} \int_0^{2\pi} d\phi \int_0^\pi d\theta \sin\theta \cos\theta | \langle e^{i(\mathbf{k}_0 - \mathbf{k}) \cdot \mathbf{r}} \rangle |^2. \quad (56)$$

Since for a spherically Gaussian distribution  $N(s_\infty - f_\infty) \approx N/(8\sigma^4) = b_0/(24\sigma^2)$ , from Eq. (52) the stationary radiation force is [3,7,8]

$$\langle \hat{F} \rangle = \hbar k_0 \Gamma \left( \frac{\Omega_0}{\Gamma} \right)^2 \frac{1 + N(s_\infty - f_\infty)}{4\delta^2 + (1 + Ns_\infty)^2} \quad (57)$$

$$\approx \hbar k_0 \Gamma \left( \frac{\Omega_0}{\Gamma} \right)^2 \frac{1 + b_0/24\sigma^2}{4\delta^2 + (1 + b_0/12)^2}. \quad (58)$$

As can be observed in Fig. 1, the STD state yields a good agreement with the full-spectrum approach and the  $N$ -body simulations only for small values of the optical thickness.

Finally, for that state Eq. (49) the scattered radiation electric field, Eq. (A5), and intensity, Eq. (25), become

$$\mathcal{E}_S(r, \theta, \phi, t) = \frac{dk_0^2}{4\pi\epsilon_0 r} e^{ik_0(r-ct)} \beta_{TD}(t) \langle e^{i(\mathbf{k}_0 - \mathbf{k}) \cdot \mathbf{r}} \rangle \quad (59)$$

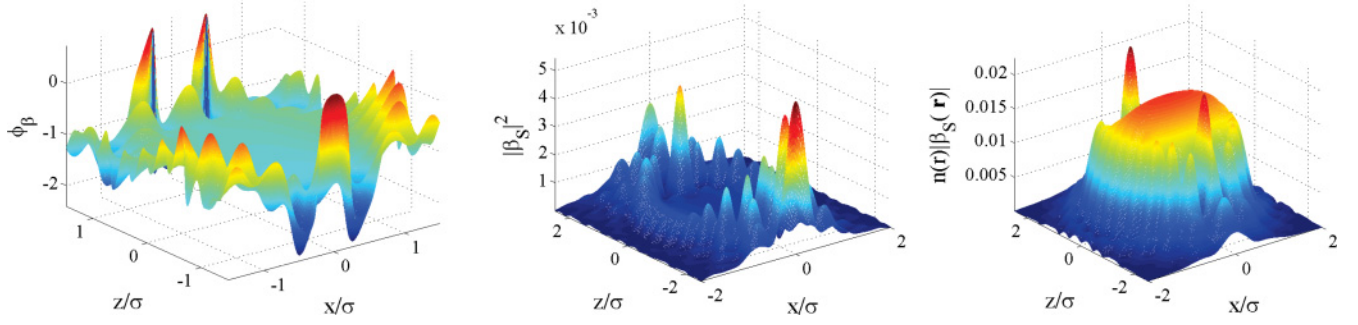


FIG. 3. (Color online) Phase  $\phi_\beta$  of the excitation amplitude  $\beta_s$  (left), Excitation probability  $|\beta_s|^2$  of the atoms in the  $(x,z)$  plane ( $y = 0$ ) (center) and contribution to the radiation of the electric field in the same plane, which corresponds to the level of excitation of the atoms weighted by their local density (right). Simulations realized using the analytic expressions (15), for  $N = 10^4$ ,  $\sigma = 10$ , and  $\delta = 10$ .

and

$$I_S(r, \theta, \phi) = c\epsilon_0 \left( \frac{dk_0^2}{4\pi\epsilon_0 r} \right)^2 |\beta_{TD}|^2 [N + N^2 |e^{i(\mathbf{k}_0 - \mathbf{k}) \cdot \mathbf{r}}|^2]. \quad (60)$$

In particular, for a Gaussian distribution,  $\langle \exp[i(\mathbf{k}_0 - \mathbf{k}) \cdot \mathbf{r}] \rangle = \exp[-\sigma^2(1 - \cos \theta)/2]$ .

Figure 3 shows the phase of the excitation amplitude  $\beta_s$  (left) and the excitation probability,  $|\beta_s|^2$  (center), in the  $(x,z)$  plane ( $y = 0$ ), calculated from the exact solution of Eq. (15), for  $N = 10^4$ ,  $\sigma = 10$ , and  $\delta = 10$ . Figure 3 (right) shows the contribution to the electric field radiation in the same plane, weighted by the local atomic density. The simplification of the STD state, as compared to the exact solution of Eq. (15), resides in the assumption that all atoms are equally excited and oscillate in phase. According to the exact calculation, the atomic dipoles appear to be in phase only in the core of the cloud (see Fig. 3, left), but this phase profile has strong distortion away from it. This phenomenon is all the more important as the atoms are much more excited in the peripheral region than in the core (see Fig. 3, center). In particular, even when this excitation probability is weighted by the particle density, two areas at the cloud entrance and exit contribute significantly to the radiation electric field of Eq. (24) (see peaked structures in Fig. 3, right). For a STD state, both the phase profile and average excitation remain flat throughout the cloud. From a macroscopic point of view, the STD state

neglects phase shifts imprinted into the pump beam by the cloud's reflective index. This can be seen in Fig. 4(a), which compares the phase of the STD state,  $\beta_{TD} \exp(i\mathbf{k}_0 \cdot \mathbf{r})$  (linear curve, no phase shift), and  $\beta_s(\mathbf{r})$  (additional phase-shift) along the optical axis across the cloud. Figure 4(b) shows the pump beam phase shift after transmission through the atomic cloud as a function of atom number. This phase shift is at the origin of the deviation between the radiation pressure forces calculated for the STD state and the exact solution. The pump beam phase shift leads to a reduction of the absorption and the emission forces. This can be understood as destructive interference of forward radiation emitted from different atoms, located at the same plane  $z = z_0$  but different  $x$  or  $y$ .

As for the emitted wave, it is concentrated in the forward direction (see Fig. 5, left), and there is no backscattering (not shown here). The wavefront phase does not exhibit significant distortion in the central region of the radiated beam (see Fig. 5, right).

## VII. CONCLUSIONS

In summary, we studied collective scattering from a dense and large atomic cloud with Gaussian density profile in terms of the eigenvalues of the interaction operator. This enabled us to calculate the state generated by the interaction with a laser beam. We found that this state considerably deviates from the ‘‘timed Dicke’’ state at high optical densities. In order to characterize this state, we calculated the phase front

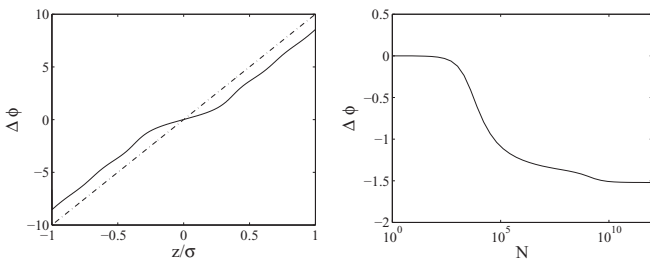


FIG. 4. Left: Phase shift along the optical axis for the exact solution (15) (plain line) and a STD state (49) (dash-dotted line). Right: Phase shift of the pump beam after transmission through the cloud as a function of  $N$  evaluated along the axis,  $x = y = 0$ , at  $k_0 z = 20\sigma$ , for  $N = 10^4$ ,  $\sigma = 10$ , and  $\delta = 10$ .

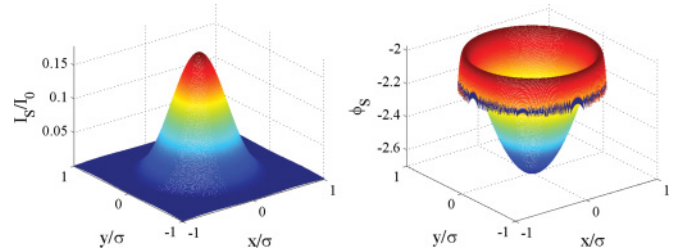


FIG. 5. (Color online) Transverse intensity profile (left) of the wave emitted by the cloud, at  $z = 3\sigma$  and its wavefront (right). Simulations realized using the analytic Eq. (24), for  $N = 10^4$ ,  $\sigma = 10$ , and  $\delta = 10$ .



of the excited atomic dipole moments and the force due to cooperative scattering by the atomic cloud.

Our approach consisted in expanding the solution on spherical harmonics, which form a complete orthogonal basis of the Hermitian interaction matrix. Under the assumption that the system is sufficiently dilute to neglect short-range effects due to dipole-dipole interactions, the continuous spectrum approximation allows to transform infinite series into solvable integrals and eventually to derive analytical expressions for the most relevant observables, such as the scattered intensity and radiation pressure force. These analytical expressions show good agreement with the numerical solution of the  $N$ -body problem and highlight the dependence on the accessible experimental parameters, such as optical thickness, atomic cloud size, and laser frequency.

The analytical solution appears particularly useful for studying the thermodynamic limit when  $N \rightarrow \infty$  and  $V \rightarrow \infty$  with  $N/V$  fixed, until collisions or nonresonant interactions come into play. The thermodynamic limit is hardly accessible to  $N$ -body simulations, since the latter are highly CPU consuming.

In contrast, the eigenvalue approach opens the possibility to study the fascinating link between microscopic and macroscopic domains of light scattering and in particular between single-atom scattering and Mie scattering for extended continuous samples [5].

For large optical thickness, the refraction index of the cloud acts back on the driving field and shifts its phase. For this reason, the solution for large optical thickness shows appreciable deviations from that obtained assuming a symmetric timed Dicke state for the atomic sample, since the latter corresponds to a completely degenerate eigenvalue spectrum. The exact solution of Eq. (15) takes into account the induced phase shift and reduces to the symmetric timed Dicke state in the limit of relatively small optical thickness.

An important further development of the present study should be to understand how the dipole-dipole interactions contribute to the observed cooperative effects, completing in this way the cooperative scattering description for highly compressed and dense atomic clouds.

#### ACKNOWLEDGMENTS

We acknowledge fruitful discussions with R. Kaiser and T. Bienaimé. We are also grateful to F. Staniscia for support for the numerical simulations. The work has been supported by the COSCALI network within the IRSES program of the European Commission under Grant No. PIRSES-GA-2010-268717.

#### APPENDIX A: DERIVATION OF THE SCATTERED ELECTRIC FIELD

The scattered radiation is provided by the positive-frequency part of the electric field operator,

$$\hat{E}_S(\mathbf{r}, t) = \sum_{\mathbf{k}} \mathcal{E}_k \hat{a}_{\mathbf{k}}(t) e^{i\mathbf{k}\cdot\mathbf{r} - i\omega_k t}, \quad (\text{A1})$$

where  $\mathcal{E}_k = (\hbar\omega_k/2\epsilon_0 V_{ph})^{1/2}$ . Integrating Eq. (5) with  $a_{\mathbf{k}}(0) = 0$ , inserting it in Eq. (A1), and approximating the sum over the modes  $\mathbf{k}$  by an integral, we obtain

$$\begin{aligned} \hat{E}_S(\mathbf{r}, t) = & -i \frac{V_{ph}}{8\pi^3} \sum_{m=1}^N \int_0^t dt' \hat{\sigma}_m(t-t') e^{i\omega_a t'} \\ & \times \int d\mathbf{k} \mathcal{E}_k g_k e^{i\mathbf{k}\cdot(\mathbf{r}-\mathbf{r}_m) - i\mathbf{k}t'}. \end{aligned} \quad (\text{A2})$$

Introducing spherical coordinates,  $d\mathbf{k} = dk k^2 d\phi d\theta \sin\theta$ , and integrating the angular part, Eq. (A2) becomes

$$\begin{aligned} \hat{E}_S(\mathbf{r}, t) = & -\frac{V_{ph}}{4\pi^2} \sum_{m=1}^N \frac{1}{|\mathbf{r}-\mathbf{r}_m|} \int_0^t dt' \hat{\sigma}_m(t-t') e^{i\omega_a t'} \\ & \times \int_0^\infty dk k \mathcal{E}_k g_k \{ e^{-i\mathbf{k}\cdot(\mathbf{r}-\mathbf{r}_m)/c} \\ & - e^{-i\mathbf{k}\cdot(\mathbf{r}'+\mathbf{r}_m)/c} \}. \end{aligned} \quad (\text{A3})$$

Assuming the radiation spectrum centered around  $k \approx k_0$ , we approximate  $k\mathcal{E}_k g_k \approx k_0 \mathcal{E}_{k_0} g_{k_0}$ . Then, extending the lower limit of integration of  $k$  to  $-\infty$ , we obtain for  $t < |\mathbf{r}-\mathbf{r}_m|/c$  [5,23]

$$\hat{E}_S(\mathbf{r}, t) \approx -\frac{dk_0^2}{4\pi\epsilon_0} \sum_{m=1}^N \frac{e^{ik_0|\mathbf{r}-\mathbf{r}_m|}}{|\mathbf{r}-\mathbf{r}_m|} \hat{\sigma}_m(t - |\mathbf{r}-\mathbf{r}_m|/c). \quad (\text{A4})$$

Neglecting the radiation retard in the limit  $t \gg \sigma_R/c$ , where  $\sigma_R$  is the cloud size, and approximating in the far field limit  $|\mathbf{r}-\mathbf{r}_m| \approx r - \hat{\mathbf{n}} \cdot \mathbf{r}_m$ , where  $\hat{\mathbf{n}} = \mathbf{r}/r$ , Eq. (A4) becomes

$$\hat{E}_S(r, \theta, \phi, t) \approx -\frac{dk_0^2}{4\pi\epsilon_0 r} e^{ik_0(r-ct) + i\Delta_0 t} \sum_{m=1}^N \hat{\sigma}_m(t) e^{-i\mathbf{k}_s \cdot \mathbf{r}_m}, \quad (\text{A5})$$

where  $\mathbf{k}_s = k_0(\sin\theta \cos\phi, \sin\theta \sin\phi, \cos\theta)$ . When applied on the state of Eq. (2), neglecting virtual transitions, it yields  $\hat{E}_S|\Psi\rangle = \mathcal{E}_S|g_1 \dots g_N\rangle$  and where  $\mathcal{E}_S$ , in the continuous density approximation will be given by Eq. (22).

#### APPENDIX B: DERIVATION OF EQ. (36)

The angular integral in Eq. (34) is

$$\begin{aligned} & \int_0^{2\pi} d\phi \int_0^\pi d\theta \sin\theta \cos\theta e^{-i\mathbf{k}\cdot(\mathbf{r}-\mathbf{r}')} \\ & = 4\pi i \frac{z-z'}{|\mathbf{r}-\mathbf{r}'|} j_1(k_0|\mathbf{r}-\mathbf{r}'|). \end{aligned} \quad (\text{B1})$$

Since

$$\frac{\partial}{\partial z} j_0(k_0|\mathbf{r}-\mathbf{r}'|) = -k_0 \frac{(z-z')}{|\mathbf{r}-\mathbf{r}'|} j_1(k_0|\mathbf{r}-\mathbf{r}'|),$$

where  $j_0(x) = \sin(x)/x$ , Eq. (34) can be written as

$$\begin{aligned} \langle \hat{F}_e \rangle = & -i \frac{\hbar k_0 \Gamma}{2N} \int d\mathbf{r} n(\mathbf{r}) \left\{ \beta(\mathbf{r}) \frac{\partial}{\partial(k_0 z)} \right. \\ & \times \left. \int d\mathbf{r}' n(\mathbf{r}') j_0(k_0|\mathbf{r}-\mathbf{r}'|) \beta^*(\mathbf{r}') - \text{c.c.} \right\}. \end{aligned} \quad (\text{B2})$$

Using the expansion Eqs. (7), (9), (8), and (11), we obtain

$$\int d\mathbf{r}' n(\mathbf{r}') j_0(k_0|\mathbf{r} - \mathbf{r}'|) \beta^*(\mathbf{r}') = \sum_{n=0}^{\infty} \sum_{m=-n}^n \alpha_{nm}^* \lambda_n j_n(k_0 r) Y_{nm}^*(\theta, \phi). \quad (\text{B3})$$

In spherical coordinates,

$$\frac{\partial}{\partial z} = \cos \theta \frac{\partial}{\partial r} + \frac{\sin^2 \theta}{r} \frac{\partial}{\partial \cos \theta},$$

and

$$\langle \hat{F}_e \rangle = -i \frac{\hbar k_0 \Gamma}{2N} \int d\mathbf{r} n(r) \left\{ \beta(\mathbf{r}) \sum_{n=0}^{\infty} \sum_{m=-n}^n \alpha_{nm}^* \lambda_n \left( \cos \theta \frac{\partial}{\partial(k_0 r)} + \frac{\sin^2 \theta}{k_0 r} \frac{\partial}{\partial \cos \theta} \right) j_n(k_0 r) Y_{nm}^*(\theta, \phi) - \text{c.c.} \right\} \quad (\text{B4})$$

Still using Eq. (9),

$$\begin{aligned} \langle \hat{F}_e \rangle &= -\frac{\hbar k_0 \Gamma}{2N} \sum_{p=0}^{\infty} \sum_{q=-p}^p \sum_{n=0}^{\infty} \sum_{m=-n}^n \lambda_n \int_0^{\infty} dr r^2 n(r) j_p(k_0 r) \int_0^{2\pi} d\phi \int_0^{\pi} d\theta \sin \theta \\ &\times \left\{ \frac{\partial j_n(k_0 r)}{\partial(k_0 r)} \cos \theta Y_{pq}(\theta, \phi) Y_{nm}^*(\theta, \phi) + \frac{j_n(k_0 r)}{k_0 r} \sin^2 \theta Y_{pq}(\theta, \phi) \frac{\partial Y_{nm}^*(\theta, \phi)}{\partial(\cos \theta)} \right\} i(\alpha_{pq} \alpha_{nm}^* - \text{c.c.}). \end{aligned} \quad (\text{B5})$$

Assuming as before

$$\alpha_{nm} = \alpha_n \delta_{m,0},$$

and since

$$Y_{n0}(\theta, \phi) = \sqrt{\frac{2n+1}{4\pi}} P_n(\cos \theta),$$

Eq. (B5) becomes

$$\begin{aligned} \langle \hat{F}_e \rangle &= -\frac{\hbar k_0 \Gamma}{4N} \sum_{p=0}^{\infty} \sum_{n=0}^{\infty} \lambda_n \sqrt{(2n+1)(2p+1)} \int_0^{\infty} dr r^2 n(r) j_p(k_0 r) \int_0^{\pi} d\theta \sin \theta \\ &\times \left\{ \frac{\partial j_n(k_0 r)}{\partial(k_0 r)} \cos \theta P_p(\cos \theta) P_n(\cos \theta) + \frac{j_n(k_0 r)}{k_0 r} \sin^2 \theta P_p(\cos \theta) \frac{\partial P_n(\cos \theta)}{\partial(\cos \theta)} \right\} i(\alpha_p \alpha_n^* - \text{c.c.}). \end{aligned} \quad (\text{B6})$$

Since

$$\int_0^{\pi} d\theta \sin \theta \cos \theta P_p(\cos \theta) P_n(\cos \theta) = \int_{-1}^1 dx x P_n(x) P_p(x)$$

and

$$\int_0^{\pi} d\theta \sin^3 \theta P_p(\cos \theta) \frac{\partial P_n(\cos \theta)}{\partial(\cos \theta)} = \int_{-1}^1 dx (1-x^2) P_p(x) \frac{d}{dx} P_n(x),$$

using the identities

$$(2p+1)x P_p(x) = (p+1)P_{p+1}(x) + pP_{p-1}(x),$$

$$(x^2-1) \frac{dP_n(x)}{dx} = n[xP_n(x) - P_{n-1}(x)],$$

and

$$\int_{-1}^1 dx P_n(x) P_p(x) = \frac{2}{2n+1} \delta_{n,p},$$

we obtain

$$\int_{-1}^1 dx x P_n(x) P_p(x) = \frac{2}{(2p+1)(2n+1)} \{(p+1)\delta_{n,p+1} + p\delta_{p,n+1}\}$$

and

$$\int_{-1}^1 dx (x^2-1) P_p(x) \frac{d}{dx} P_n(x) = \frac{2n}{(2n+1)(2p+1)} \{p\delta_{p,n+1} - (n+1)\delta_{n,p+1}\}.$$

By substituting these expressions in Eq. (B6), we obtain

$$\langle \hat{F}_e \rangle = -\frac{\hbar k_0 \Gamma}{2N} \sum_{p=0}^{\infty} \sum_{n=0}^{\infty} i(\alpha_p \alpha_n^* - \text{c.c.}) \frac{\lambda_n}{\sqrt{(2n+1)(2p+1)}} \int_0^{\infty} dr r^2 n(r) j_p(k_0 r) \\ \times \left\{ (p+1) \left[ \frac{\partial j_{p+1}(k_0 r)}{\partial(k_0 r)} + (p+2) \frac{j_{p+1}(k_0 r)}{k_0 r} \right] \delta_{n,p+1} + p \left[ \frac{\partial j_n(k_0 r)}{\partial(k_0 r)} - n \frac{j_n(k_0 r)}{k_0 r} \right] \delta_{p,n+1} \right\}. \quad (\text{B7})$$

Since

$$\frac{dj_{n+1}(z)}{dz} = j_n(z) - \frac{n+2}{z} j_{n+1}(z),$$

and

$$\frac{dj_n(z)}{dz} = -j_{n+1}(z) + \frac{n}{z} j_n(z),$$

using the definition Eq. (11),

$$\langle \hat{F}_e \rangle = -\frac{\hbar k_0 \Gamma}{8\pi N} \sum_{p=0}^{\infty} \sum_{n=0}^{\infty} i(\alpha_p \alpha_n^* - \text{c.c.}) \frac{\lambda_n \lambda_p}{\sqrt{(2n+1)(2p+1)}} \{(p+1)\delta_{n,p+1} - p\delta_{p,n+1}\}. \quad (\text{B8})$$

Eliminating one of the two sums, we obtain

$$\langle \hat{F}_e \rangle = -\frac{\hbar k_0 \Gamma}{4\pi N} \sum_{n=0}^{\infty} \frac{(n+1)\lambda_n \lambda_{n+1}}{\sqrt{(2n+1)(2n+3)}} i(\alpha_n \alpha_{n+1}^* - \text{c.c.}). \quad (\text{B9})$$

In the stationary case,

$$\alpha_n = \frac{\Omega_0 i^n \sqrt{4\pi(2n+1)}}{\Gamma 2\delta + i(1+\lambda_n)},$$

and the stationary force is

$$\langle F_e \rangle = -\hbar k_0 \frac{2\Omega_0^2}{\Gamma N} \sum_{n=0}^{\infty} \frac{(n+1)\lambda_n \lambda_{n+1} [4\delta^2 + (1+\lambda_n)(1+\lambda_{n+1})]}{[4\delta^2 + (1+\lambda_n)^2][4\delta^2 + (1+\lambda_{n+1})^2]}. \quad (\text{B10})$$

- 
- [1] R. H. Dicke, *Phys. Rev.* **93**, 99 (1954).  
[2] M. O. Scully, E. S. Fry, C. H. Ooi, and K. Wodkiewicz, *Phys. Rev. Lett.* **96**, 010501 (2006).  
[3] P. W. Courteille, S. Bux, E. Lucioni, K. Lauber, T. Bienaimé, R. Kaiser, and N. Piovella, *Eur. J. Phys. D* **58**, 69 (2010).  
[4] H. C. van de Hulst, *Light Scattering by Small Particles* (Dover Publications, New York, 1981).  
[5] S. Prasad and R. J. Glauber, *Phys. Rev. A* **82**, 063805 (2010).  
[6] A. A. Svidzinsky, J. T. Chang, and M. O. Scully, *Phys. Rev. A* **81**, 053821 (2010).  
[7] T. Bienaimé, S. Bux, E. Lucioni, P. W. Courteille, N. Piovella, and R. Kaiser, *Phys. Rev. Lett.* **104**, 183602 (2010).  
[8] H. Bender, C. Stehle, S. Slama, R. Kaiser, N. Piovella, C. Zimmermann, and P. W. Courteille, *Phys. Rev. A* **82**, 011404 (2010).  
[9] R. Bonifacio, L. De Salvo, L. M. Narducci, and E. J. D'Angelo, *Phys. Rev. A* **50**, 1716 (1994).  
[10] S. Slama, G. Krenz, S. Bux, C. Zimmermann, and P. W. Courteille, *Phys. Rev. A* **75**, 063620 (2007).  
[11] S. Inouye, A. P. Chikkatur, D. M. Stamper-Kurn, J. Stenger, D. E. Pritchard, and W. Ketterle, *Science* **285**, 571 (1999).  
[12] L. Fallani, C. Fort, N. Piovella, M. M. Cola, F. S. Cataliotti, M. Inguscio, and R. Bonifacio, *Phys. Rev. A* **71**, 033612 (2005).  
[13] M. G. Moore, O. Zobay, and P. Meystre, *Phys. Rev. A* **60**, 1491 (1999).  
[14] S. Bux, Ch. Gnaahm, R. A. W. Maier, C. Zimmermann, and P. W. Courteille, *Phys. Rev. Lett.* **106**, 203601 (2011).  
[15] R. Friedberg, S. R. Hartman, and J. T. Manassah, *Phys. Rep.* **7**, 101 (1973).  
[16] A. A. Svidzinsky, J. T. Chang, and M. O. Scully, *Phys. Rev. Lett.* **100**, 160504 (2008).  
[17] M. Abramowitz and I. A. Stegun, in *Handbook of Mathematical Functions* (Dover, New York, 1972), p. 377.  
[18] I. S. Gradshteyn and I. M. Ryzhik, in *Table of Integrals, Series, and Products* (Elsevier Academic Press, San Diego, 2007), p. 885.  
[19] M. O. Scully and A. A. Svidzinsky, *Phys. Lett. A* **373**, 1283 (2009).  
[20] M. O. Scully and A. A. Svidzinsky, *Science* **328**, 1239 (2010).  
[21] R. Röhlberger, K. Schlage, B. Sahoo, S. Couet, and R. Ruffer, *Science* **328**, 1239 (2010).  
[22] A. A. Svidzinsky and M. O. Scully, *Opt. Commun.* **282**, 2894 (2009).  
[23] R. Loudon, in *The Quantum Theory of Light*, 2nd ed. (Clarendon Press, Oxford, 1983), p. 205.